Journal of Alloys and Compounds 502 (2010) 169–175

Contents lists available at ScienceDirect

Journal of Alloys and Compounds

journal homepage: www.elsevier.com/locate/jallcom

Synthesis, magnetic and electrical properties of Fe-containing SiO_2 nanocomposite

E. Thirumal [a], D. Prabhu [b], K. Chattopadhyay [b], V. Ravichandran [a,*]

[a] Materials Science Centre, Department of Nuclear Physics, University of Madras, Guindy Campus, Chennai 600 025, India
[b] Department of Materials Engineering, Indian Institute of Science, Bangalore 560 012, India

ARTICLE INFO

Article history:
Received 9 November 2009
Received in revised form 20 April 2010
Accepted 23 April 2010
Available online 18 May 2010

Keywords:
Composite materials
Chemical synthesis
Dielectric response
Oxidation
Thermal analysis
Electrochemical impedance spectroscopy

ABSTRACT

Nanocrystalline Fe powders were synthesized by transmetallation reaction and embedded in silica to form Fe–SiO_2 nanocomposite. Thermomagnetic study of the as-prepared Fe sample indicates the presence of Fe_3O_4 and Fe particles. Oxidation studies of Fe and Fe–SiO_2 show an increased thermal stability of Fe–SiO_2 nanocomposite over pure Fe. The Fe–SiO_2 shows an enhanced oxidation temperature (i.e., 780 K) and a maximum saturation magnetization value of (135 emu/g) with 64 wt.% of Fe content in silica. Electrical and dielectric behaviour of the Fe–SiO_2 nanocomposite has been investigated as a function of temperature and frequency. Low frequency ac conductivity and dielectric constants were found to be influenced by desorptions of chemisorbed moisture. High saturation magnetization, thermal stability, frequency-dependent conductivity and low power loss make Fe–silica a promising material for high frequency applications.

1. Introduction

Magnetic metal and alloy nanoparticles encapsulated in non-magnetic metals, insulators, ferrites and polymers have attracted great interest due to their potential applications in high frequency transformers, inductive components [1], magneto impedance, microwave absorber [2], etc. Among various magnetic materials, nanocrystalline Fe gains attention due to its high saturation magnetization, permeability and low coercivity. However, Fe particles in nano form have a high affinity for oxygen. Despite the reduction of their total magnetic moment, when dispersed in non-magnetic matrix or coating, several studies have been conducted to encapsulate these particles in silica [1,3], alumina [4], yittria [5,6], gold [7], carbon [8], boron nitride [9], and Fe_3O_4 [10,11] in order to improve their stability, electrical and magnetic properties. Fe–silica nanocomposites are of particular interest because they have higher resistivity and this combined with the good magnetic properties of metallic Fe, makes them a good candidate for dielectric applications and could possibly be a good replacement material for ferrites.

In this work we have synthesized nanocrystalline Fe particles by transmetallation chemical method and their composite with amorphous silica by sol–gel reaction method. Thermal stability and magnetic properties of native and Fe–silica nanocomposite have been studied. The ac electrical and dielectric behaviour of Fe–SiO_2 nanocomposite have been investigated using impedance spectroscopy.

2. Experimental method

2.1. Materials

Merck products of anhydrous $FeCl_3$ analytical reagent (96%), aluminium fine metal powder 200 mesh (99.7%), sodium hydroxide (98%), 25% NH_3 ammonia solution, Hong-Yang Chemical product of Ethanol (99.9%) and Aldrich tetraethyl orthosilicate (TEOS) (98%) were purchased and used without further purification.

2.2. Methods

For the synthesis of nanocrystalline Fe particles by transmetallation chemical method, typically, 8.4 g anhydrous $FeCl_3$ was added to 100 ml of distilled water. After the mixture was stirred for 10 min to form a homogeneous solution, 3 g of fine aluminium powder was added to the solution with constant stirring and within a few minutes a vigorous exothermic reaction was observed. After the completion of the reaction, a black precipitation of Fe powder was obtained and the temperature of the solution increased from room temperature to 340 K. The precipitates were repeatedly washed with distilled water in order to remove the byproducts such as $AlCl_3$, etc. Further, to remove the unreacted aluminium particles, the precipitates were repeatedly washed with 0.5 M NaOH solution followed by distilled water. The obtained black powders were washed and stored in ethanol.

In order to prepare Fe–silica nanocomposite, certain quantity of Fe powder was dispersed in 100 ml ethanol. Then 30 ml of 10 vol.% TEOS in ethanol solution was slowly added to it with mechanical stirring and finally 25 ml of 5 vol.% of ammonia (25% NH_3 in H_2O) in ethanol solution was also added slowly. The stir-

* Corresponding author.
Tel.: +91 44 22202800/22351444; fax: +91 44 22570305/44 22352494.
E-mail addresses: es_thirumal@yahoo.com (E. Thirumal), ravichandranvraman@gmail.com (V. Ravichandran).

0925-8388/$ – see front matter © 2010 Elsevier B.V. All rights reserved.
doi:10.1016/j.jallcom.2010.04.135

ring was continued for 12 h and aged for 48 h. The resulting Fe–silica composite powders was washed with acetone and dried in air for 1 h at 350 K. The phase purity of Fe and Fe–silica composite particles were studied by X-ray diffraction (XRD) with Bragg–Brentano configuration using Cu Kα radiation. Room temperature hysteresis loops were recorded using a vibrating sample magnetometer (VSM; EG&G Princeton Applied research 4500 model). Oxidation behaviour and thermomagnetic studies were performed by thermogravimetric analysis (TGA) using PerkinElmer instruments. The microstructures of the materials were studied using scanning electron microscopy (SEM; with a JEOL JSM 840 model) and transmission electron microscopy (TEM; of JEOL FX2000). Particle size distribution was measured using dynamic light scattering (DLS) at room temperature with a Zetasizer 3000HSA (Malvern Instruments, UK). Fourier transform of infra-red (FT-IR) spectra were recorded in the transmission mode for Fe–SiO_2 nanocomposite with an FT-IR spectrometer (PerkinElmer). Using hydraulic pressure (Lawrence & Mayo (India) Pvt. Ltd. (Model: LM-17-510)), powder Fe–silica sample was compacted in the form of a pellet with applied pressure of 4975 kg/cm^2. Electrical conductivity and dielectric properties were measured as a function of frequency in the range of 1 Hz–10 MHz, using an impedance gain/phase analyzer (Solertron 1260) interfaced to a personal computer.

3. Results and discussion

Fig. 1 presents the XRD pattern of the pure and Fe–silica composite. It could be observed that the as-prepared Fe particles have pure BCC structure with high crystallinity. The intensity ratios as well as peak positions (Miller indices) which correspond to 44.69° (1 1 0), 65.07° (2 0 0) and 82.38° (2 1 1) match very well with JCPDS card No.: 87-0721. The average crystallite size of the as-prepared powder, calculated using Scherrer formula including the correction for instrumental broadening, was found to be about 50 nm. Oxide phases were not observed by means of XRD and hence the oxide layer on Fe particles may be in amorphous form. The XRD pattern of Fe particles encapsulated with silica also exhibit the peak positions of BCC-Fe structure. Absence of peaks corresponding to silica indicates the formation of amorphous silica. In order to identify the presence of silica in Fe–SiO_2 nanocomposite, the samples were examined by SEM analysis. Fig. 2(a) is the bright field TEM micrographs showing typical Fe crystallites about 50 nm in size and Fig. 2(b) is the bright field image showing such crystallites

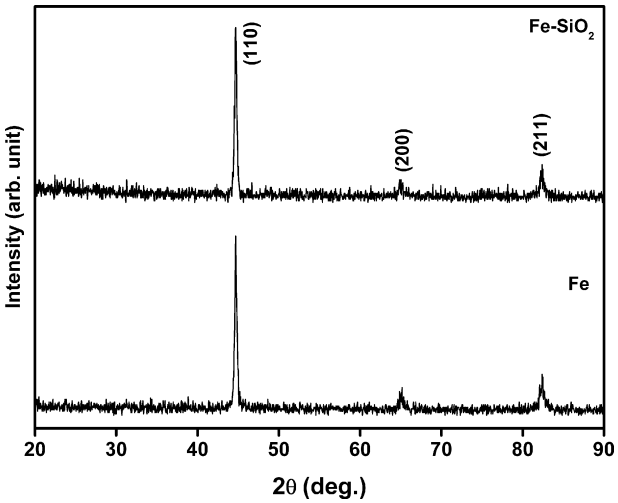

Fig. 1. Powder XRD pattern showing high crystallinitiy of the as-prepared Fe and Fe–silica nanocomposite.

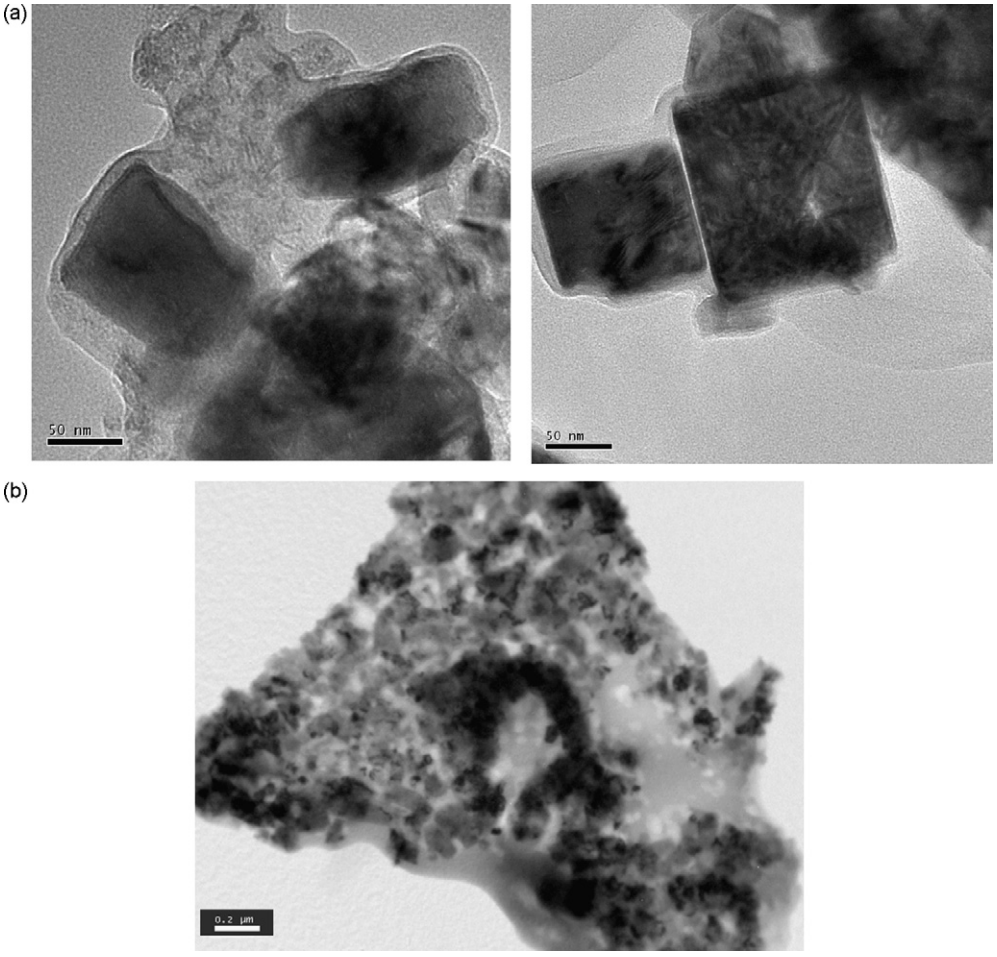

Fig. 2. Bright field TEM images showing (a) native Fe crystallites with typical grain sizes of about 50 nm, (b) Fe crystallites dispersed in a silica matrix.

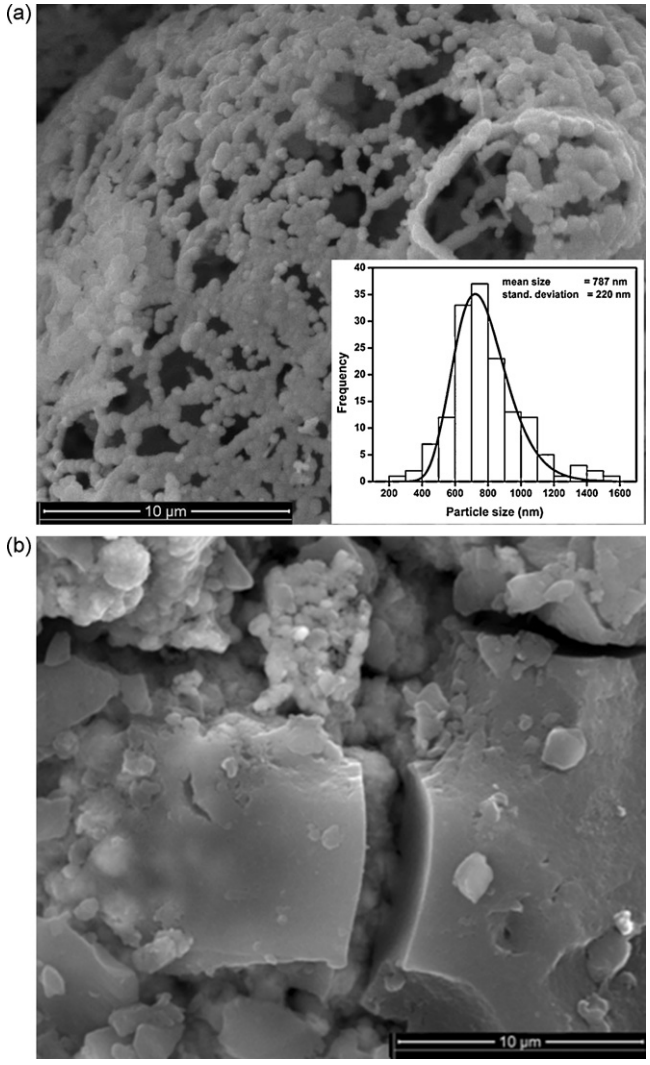

Fig. 3. SEM microstructure of (a) as-prepared Fe particles with hollow spherical morphology made of network of Fe particles with inset giving the particle size distribution, (b) Fe particles embedded in a silica matrix.

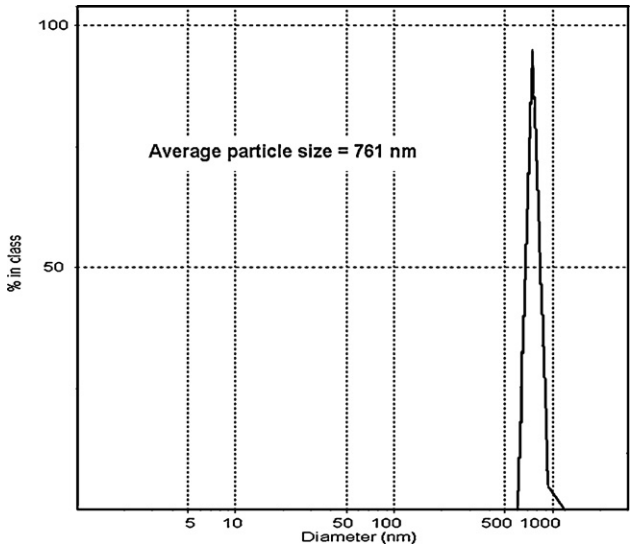

Fig. 4. Dynamic light scattering (DLS) plot of Fe particles suspended in ethanol.

embedded in an SiO_2 matrix. Fig. 3(a) and (b) are SEM micrographs showing the actual morphology of Fe and Fe–silica composite with scale bar of 10 μm. Pure Fe powder samples have hollow spherical structures made up of network of particles which have typically about a micron in size. The particle size distribution measured from SEM image is shown in the inset of Fig. 3(a). The particle distribution was fitted with a lognormal function with a mean size of 787 nm. Fig. 3(b) is the microstructure of the Fe–silica composite, which shows the presence of thick non-magnetic silica encapsulated with Fe particles.

The dynamic light scattering (DLS) experiment was carried out in order to understand the dispersion of Fe particles in EtOH medium before the silica coating process. Fig. 4 shows the particle size distribution of the Fe sample dispersed in EtOH. The average particle size was determined to be 761 nm, in good agreement with the result obtained using scanning electron microscopy. It is clear that these large particles (~750 nm) making up the network of hollow sphere are typically aggregates of Fe crystallites (~50 nm).

To confirm the presence of silica on Fe particles, the materials were also characterized by FT-IR. The IR spectrum of the composite shown in Fig. 5 exhibits a broad envelope in the higher energy region. This is due to the –OH and C–H stretching vibrations of water and ethanol molecules, which is confirmed by the bending vibrations at about 1630 cm^{-1}. Another broad band in the low energy region of the spectrum due to the characteristic vibrations of Si–O–Si is observed in the range of 960–1280 cm^{-1}. An additional sharp peak around 785 cm^{-1} suggests the presence of Si–O–Fe bonds. The band at 694 cm^{-1} is attributed to the Fe–O–Fe bond from Fe_2O_3 as described elsewhere [12]. The FT-IR spectrum indicates the presence of surface oxidation on Fe particles. Silica coating is more compatible with iron oxide molecules rather than with bare Fe atom. The vibration bond around 785 cm^{-1} indicates that the silica molecules are bonded with Fe atom through the Si–O–Fe interface layer.

Fig. 6 shows the thermogravimetric curves of Fe and Fe–SiO_2 powders obtained in the temperature range of 320–1073 K with the heating rate of 10 K/min. The nanocrystalline Fe shows a small initial weight loss of about 2.5% in the temperature range of 310–450 K, which can be attributed to the hydroxide impurities on the Fe particles. Also the curve shows a gain in weight, which begins at 554 K and increases with temperature up to 1005 K with maximum percentage of 32.5 wt.%. Hence, according to the $3Fe + 2O_2 \rightarrow Fe_3O_4$ reaction, a weight gain of only 27.6% is expected.

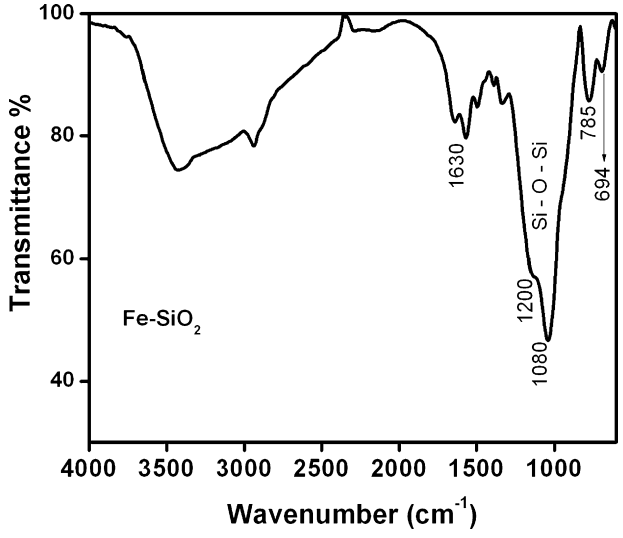

Fig. 5. The FT-IR spectrum of the as-prepared Fe–SiO_2 nanocomposite showing the presence of surface oxidation of Fe particles which makes it compatible for SiO_2 coating.

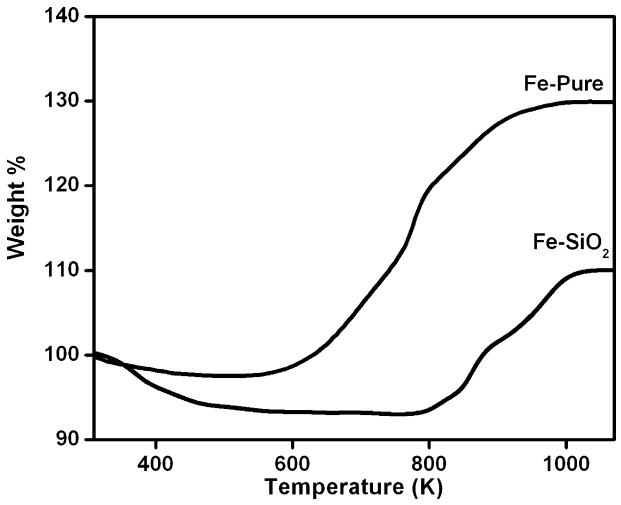

Fig. 6. Thermogravimetric oxidation curves of the as-prepared Fe and Fe–silica showing the enhanced thermal stability of the Fe–silica nanocomposite.

The observed 32.5% can be due to the formation of Fe_2O_3 by the reaction $2Fe + (3/2)O_2 \rightarrow Fe_2O_3$ which would give rise to a weight gain of 30%.

In the case of as-prepared Fe–silica, the initial weight loss of the sample from 320 K to 450 K can be attributed to the removal of water and ethanol present in the sample. With further increase in temperature there is no significant weight loss, but in the temperature range of 780–1044 K, a drastic weight gain of 17% was observed. The maximum weight gain of 17% observed for Fe–silica sample indicates the presence of oxide silica, which will not contribute to weight gain. The onset of weight gain at 780 K clearly indicates the oxidation temperature of Fe particles in the SiO_2 matrix. The observed oxidation temperature of our Fe–SiO_2 sample is much higher than the previously reported oxidation temperature of 470 K for Fe/silica core–shell structure prepared by high temperature hydrogen atmosphere reduction method [2]. The high thermal stability and enhancement in oxidation temperature of our sample can be attributed to the thick insulating silica shell covering the Fe particles. A further increase in temperature shows saturation in the weight of the sample, which indicates the formation of stable iron oxide phases such as FeO, Fe_3O_4 and Fe_2O_3.

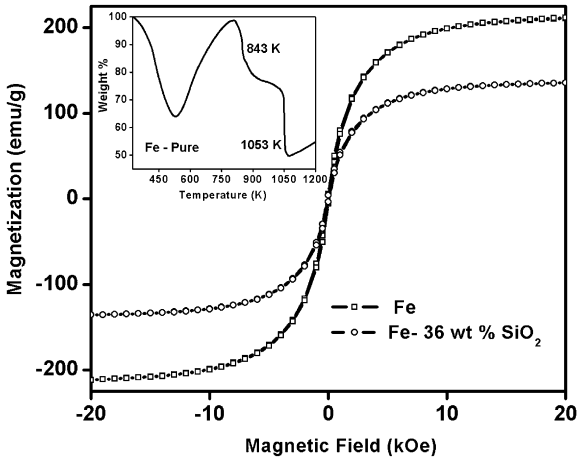

Fig. 7. Room temperature hysteresis loop of native and silica-coated Fe particles with the latter showing a reduced magnetization due to the presence of silica. (Inset) Magnetic TG plot of the as-prepared nanocrystalline Fe showing the Curie transition of Fe_3O_4 and Fe at 843 K and 1053 K respectively.

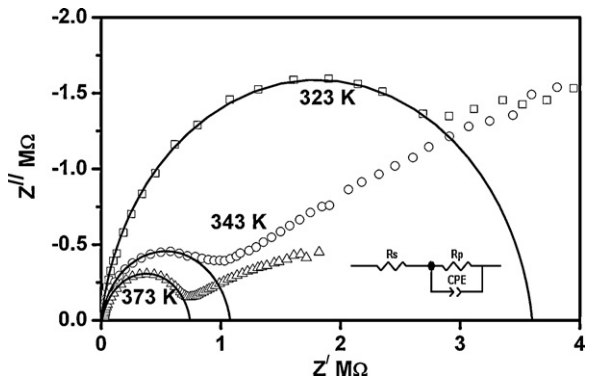

Fig. 8. Complex impedance spectra for Fe–silica nanocomposite measured at indicated temperatures with inset showing the equivalent circuit for the fitted solid line.

Fig. 7 presents the room temperature hysteresis loop of the as-prepared Fe and Fe–silica powders. The saturation magnetization (M_s) of pure Fe particles is found to be 210 emu/g, which is very close to that of the bulk Fe (220 emu/g) and in the case of Fe–silica particles it is found to be 135 emu/g of M_s. This difference in the value of the saturation magnetization enables us to estimate the presence of Fe particles as 64 wt.% in silica matrix regardless of OH and other removable molecules. In the case of the Fe–SiO_2 nanocomposite, the saturation magnetization is found to be four times higher than the values reported by Zhao et al. [13,14] and also 27% lower than that reported by Tang et al. [15]. It is evident that the high concentration of silica (36 wt.%) is the main factor to reduce the value of the saturation magnetization. The coercivity values of both Fe and Fe–SiO_2 are found to be 56 Oe. The absence of change in coercivity for silica-coated Fe particles can be attributed to several reasons. One of the main reasons is that the Fe particles may not be well separated in silica-coated Fe. However, lower coercivity of Fe and Fe–silica indicates a soft magnetic behaviour.

To find out the Curie transition temperature and identify the trace oxidation, thermomagnetic measurement was carried out on the as-prepared Fe powder. Inset in Fig. 7 shows the thermomagnetic behaviour of the as-prepared nanocrystalline Fe particles measured at temperatures ranging from 320 K to 1200 K with a constant heating rate (10 K/min) and flow of N_2 gas. The thermomagnetic plot reveals the presence of the Fe_3O_4 phase with the Curie transition at 843 K, followed by a Curie transition of metallic BCC-Fe phase at 1053 K. Cao et al. [16] have examined the thermomagnetic behaviour of amorphous Fe_2O_3 and have seen an initial decrease and rise in magnetization due to crystallization of these oxides. Our thermomagnetization also shows a similar behaviour which could be attributed to the formation of thin layer of oxides around the Fe particles as they are very prone to oxidation.

Fig. 8 illustrates the typical complex impedance plots of Fe–silica pellet (with a thickness of 1.1 mm and a diameter of 8 mm) measured at different temperatures. The *Z*-plots show the presence of a single semicircle in the higher frequency region followed by a spike in the lower frequency region. This semicircle can be attributed to the grain interior conduction followed by interfacial conduction in the Fe–silica nanocomposite. It can be seen that the diameter of the semicircle decreases with temperature, which indicates the increase of conductivity with temperature. The resistances were obtained by fitting the data, using the equivalent circuit containing a series resistance (R_s) which is connected to a parallel combination of a resistance (R_p) and a constant phase element (CPE) as shown in inset of Fig. 8. The series resistance (R_s) can be obtained from the

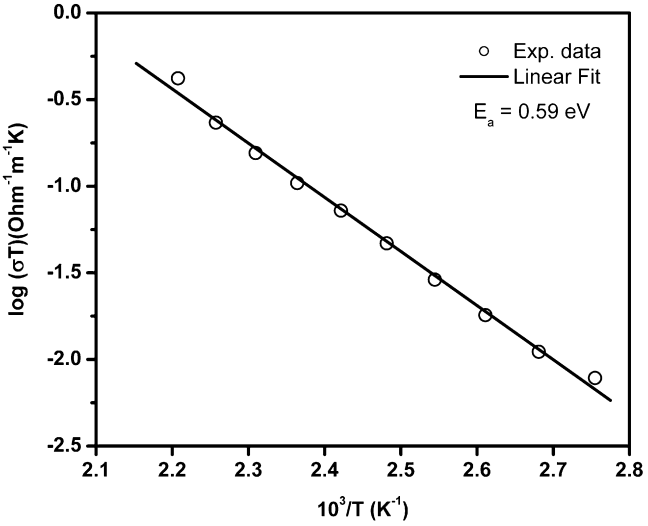

Fig. 9. Plot showing the Arrhenius behaviour of dc conductivity of the Fe–silica nanocomposite. The activation energy is determined to be 0.59 eV from the linear fit using the Arrhenius relation (Eq. (1)).

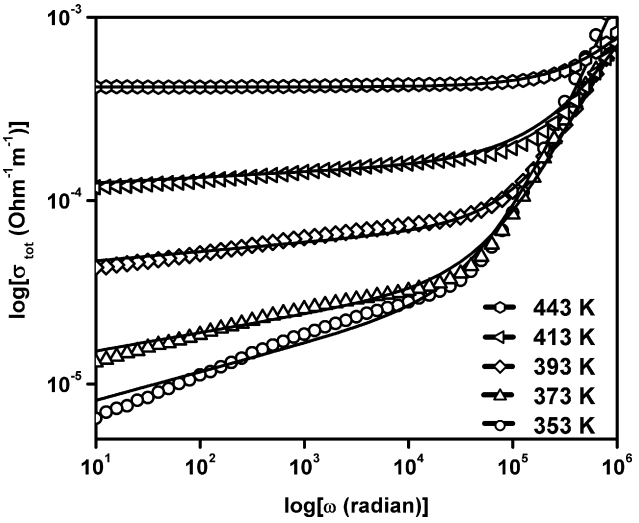

Fig. 10. Frequency spectra of ac conductivity (symbols) in the case of Fe–silica nanocomposite at different temperatures. Solid lines are the best fit for Eq. (4) for 353 K, 373 K and 393 K and Eq. (3) for 413 K and 443 K.

shift of the semicircle from the origin of plot, which is in the range of a few hundred Ohm to a few kilo-Ohm. In the case of a parallel R_p–C_p circuit, in order to analyze the depressed or more flattened semicircles, CPE has been used rather than pure capacitance. The CPE capacitance is defined as $C(\omega) = A(j\omega^{n-1})$ [17,18], where the parameter A is a constant for a given experiment. The power exponent (n) lies in between 0 and 1. The impedance of CPE behaves as pure capacitance for $n = 1$ and pure resistance for $n = 0$. The solid lines in Fig. 8 were obtained by the best fitting of non-linear least square (NLLS) fitting routine. In our case the n values fall in the range of 0.88–0.92, which are directly related to the percentage of depression of the semicircle, indicating that it is a non-ideal Debye system. Many reasons (such as rough interface between electrode and sample, presence of humidity, etc.) were suggested for the non-Debye CPE behaviour of the sample [19,20]. In our sample the presence of moisture such as –OH and –C–H molecules can be a main factor for the depressed semicircle. The obtained resistivity values lie in between 0.164 MΩ m and 1.9 kΩ m for temperatures in the range of 320–453 K.

Fig. 9 shows the temperature dependence of dc conductivity of as-prepared Fe–SiO_2 nanocomposite in the temperature range from 363 K to 453 K. The conductivity of the materials follows the Arrhenius behaviour, i.e.,

$$\sigma T = \sigma_0 \exp\left(\frac{-E_a}{kT}\right) \quad (1)$$

where σ_0 is the pre-exponential factor, E_a is the activation energy, k is the Boltzmann constant, and T is the temperature in Kelvin [21,22]. The activation energy (E_a) of the thermally activated electronic conduction in Fe–silica nanocomposite is found to be 0.59 eV, which is higher than that of Fe–Fe_3O_4–SiO_2 gel nanocomposite reported by Das et al. [11]. They observed that with an increase in the surface oxidation of the Fe particles, the activation energy of the nanocomposite decreases. In the present study the high value of activation energy 0.59 eV indicates the reduced surface oxidation, which can be attributed to complete coating of amorphous silica around the Fe particles.

Fig. 10 illustrates the ac conductivity as a function of frequency for various temperatures. It can be seen that two different ac conductivity dispersions are present in the lower temperature region. The plateau region is not observed in the temperature range of 323–423 K. Further increase in the temperature leads to a separation of the dc conductivity region and ac conductivity region, with enhanced critical frequency. According to the Almond and West dispersive behaviour the ac conductivity can be expressed as,

$$\sigma = \sigma_{dc} + A\omega^n = \sigma_{dc}\left[1 + \left(\frac{\omega}{\omega_p}\right)^n\right] \quad (2)$$

which is also called the universal power law [23]. The value of frequency exponent, n lies between 0 and 1 and the parameter A is independent of frequency. The above equation is general and universally found for semiconductors, ceramics and electronic conductors. The equation can be written as,

$$\sigma_{ac} = \sigma_{dc} + [(\omega\tau)^n](\sigma_{dc}), \qquad \sigma_{ac} = \sigma_{dc}[1 + (\omega\tau)^n] \quad (3)$$

where τ is the relaxation time.

In the present study for low frequency ac conductivity, the above equation can be modified as,

$$\sigma_{ac} = \sigma_{dc}[(\omega\tau_1)^{n_1} + (\omega\tau_2)^{n_2}] \quad (4)$$

where n_1 and n_2 are the power law exponents for low and high frequency conducting behaviour respectively; τ_1 and τ_2 are relaxation time for low and high frequency region respectively. Also $\tau_1 = 1$ s for low frequency range, whereas τ_2 will vary depending upon the critical frequency transition from the low frequency region to the high frequency region. Fig. 10 shows the measured frequency-dependent ac conductivity plots with the best fitting with Eq. (4). The n_1 value linearly decreases from 0.15 to zero when the temperature increases from 353 K to 443 K. This indicates that at lower temperatures intra-grain conduction dominates in the low frequency region. Above 443 K, the low frequency conducting dispersion behaviour disappears, which can be due to the absence of intra-grain conduction. This is mainly attributed to the presence of –OH and C–H molecules in our sample, which is also confirmed by the weight loss in the TGA measurements. Hence, above 443 K, this moisture was completely de-absorbed from the sample and the ac conductivity obeys the universal power law (Eq. (3)). At high frequencies, the strong dispersion of conduction behaviour can be due to grain interior conduction by tunneling of electrons through the dielectric barrier, a characteristic feature observed in most of the disordered materials [24,25].

Fig. 11 demonstrates the ac conductivity as a function of temperature for various frequencies. It can be observed that at lower

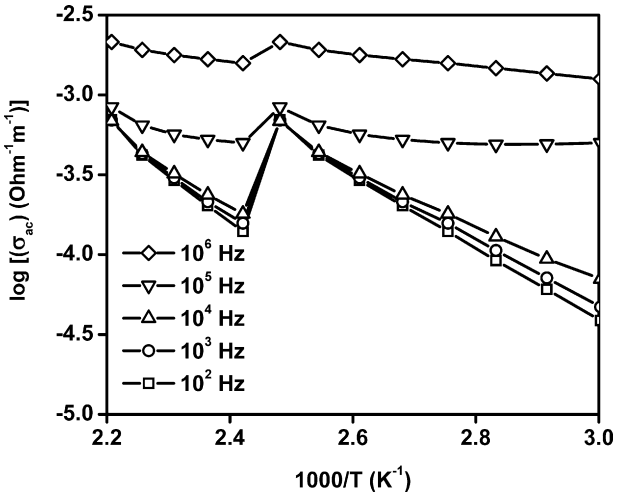

Fig. 11. Variation of ac conductivity of Fe–silica nanocomposite with temperature at different frequencies showing the strong influence of temperature on conductivity at low temperatures.

frequencies, the conductivity is strongly influenced by temperature rather than at higher frequencies. All the plots show a kink around 413 K, which can be attributed to removal of moisture from the sample.

Fig. 12(a) shows the variation of the dielectric constant of Fe–silica nanocomposite as a function of temperature at different frequencies. It is observed that at lower frequencies the value of the dielectric constant (ε') increases up to 363 K and then slightly decreases upto 403 K followed by a steep fall at 413 K, which can be attributed to thermal desorption of removable molecules. However, in the higher frequency regions (10^4 Hz, 10^5 Hz and 10^6 Hz) almost stable dielectric constant was observed except for a small change at 413 K, which indicates that the dielectric constant in the low frequency region is strongly influenced by thermal desorption compared to its behaviour in the high frequency region, as observed in the conductivity spectra. The maximum dielectric constant of bulk SiO_2 is 3.5 and nano-sized amorphous SiO_2 is 5–35 [26]. The high value of the dielectric constant in this composite material could be due to a large volume fraction of (64 wt.%) Fe embedded in silica matrix, as was observed in epoxy resin [27] and in some polymer matrix [28].

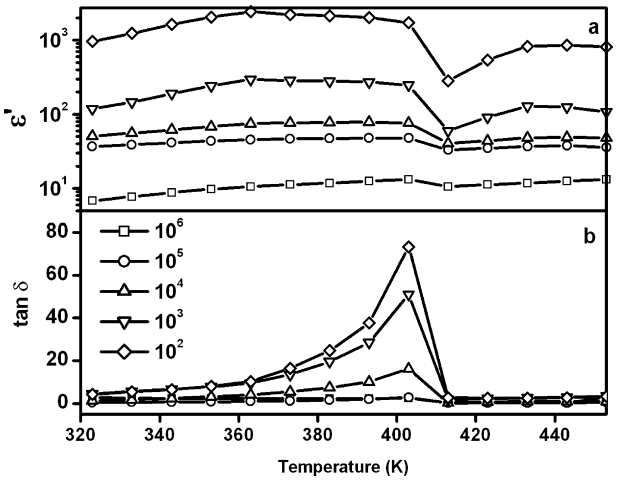

Fig. 12. Plot showing (a) dielectric constant and (b) dielectric loss of Fe–silica nanocomposite as a function of temperature measured at different frequencies.

Fig. 12(b) illustrates the dielectric loss factor ($\tan\delta$) for Fe–silica nanocomposite as a function of temperature measured at various frequencies. There is no significant change in dielectric loss in the higher frequency region (10^5 Hz and 10^6 Hz), whereas larger dielectric loss is observed in the lower frequency region (10^2 Hz, 10^3 Hz and 10^4 Hz). A sharp rise in $\tan\delta$ was observed at a thermal desorption temperature of 413 K and further increase in temperature led to a fall of the dielectric loss value below 5. Unlike ferrites, in which the dielectric loss increases with temperature [29], the Fe–silica nanocomposite exhibits almost a constant $\tan\delta$ in the higher temperature region.

4. Conclusion

We have successfully prepared magnetic metal Fe nanocrystalline powders by a simple and cost effective technique and these particles were encapsulated with silica. Analysis of particle and crystal size of Fe powder shows that our method is more suitable for synthesis of submicron size Fe particles with crystallite size of 50 nm. Fe particles dispersed in silica exhibits a clearly enhanced thermal stability. The material shows a high value of saturation magnetization and low value of electrical conductivity. Temperature dependent dielectric constant and dielectric loss indicate the suitability of this material for high frequency core materials. The amorphous silica on Fe particles may be effective in reducing the eddy current losses at high frequencies.

Acknowledgments

The authors would like to thank Prof. A. Narayanasamy, Prof. P.R. Subramaniyan, Dr R. Murugaraj, Mr. Ashok Kumar Baral and Mrs. Kalavathi for fruitful discussions. The work is supported by UGC-SAP and DST-FIST, Government of India. One of the authors DP would like to thank the Indian Institute of Science, for the award of Research Associateship.

Appendix A. Supplementary data

Supplementary data associated with this article can be found, in the online version, at doi:10.1016/j.jallcom.2010.04.135.

References

[1] Y. Zhao, X. Zhang, J.Q. Xiao, Adv. Mater. 17 (2005) 915.
[2] X.G. Liu, D.Y. Geng, Z.D. Zhang, Appl. Phys. Lett. 92 (2008) 243110.
[3] X.F. Zhang, X.L. Dong, H. Huang, B. Lv, X.G. Zhu, J.P. Lei, S. Ma, W. Liu, Z.D. Zhang, Mater. Sci. Eng. A 454 (2007) 211.
[4] F. Jay, V. Gauthier, S. Dubois, J. Am. Ceram. Soc. 89 (2006) 3522.
[5] R. Pozas, M. Ocana, M.P. Morales, C.J. Serna, Nanotechnology 17 (2006) 1421.
[6] J.R. Liu, M. Itoh, K. Machida, Chem. Lett. 32 (2003) 394.
[7] S.J. Cho, B.R. Jarrett, A.Y. Louie, S.M. Kauzlarich, Nanotechnology 17 (2006) 640.
[8] Z.D. Zhang, J.G. Zheng, I. Skorvanek, G.H. Wen, J. Kovac, F.W. Wang, J.L. Yu, Z.J. Li, X.L. Dong, S.R. Jin, W. Liu, X.X. Zhang, J. Phys.: Condens. Matter 13 (2001) 1921.
[9] H. Tokoro, S. Fujii, T. Oku, IEEE Trans. Magn. 39 (2003) 2761.
[10] O.B. Miguel, P. Tartaj, M.P. Morales, P. Bonville, U.G. Schindler, X.Q. Zhao, S.V. Verdaguer, Small 2 (2006) 1476.
[11] D. Das, S. Roy, J.W. Chen, D. Chakravorty, J. Appl. Phys. 91 (2002) 4573.
[12] S.L. Tie, H.C. Lee, Y.S. Bae, M.B. Kim, K. Lee, C.H. Lee, Colloid Surf. A: Physicochem. Eng. Aspects 293 (2007) 278.
[13] W. Zhao, J. Gu, L. Xia, H. Chen, J. Shi, J. Am. Chem. Soc. 127 (2005) 8916.
[14] S. Wang, H. Cao, F. Gu, C. Li, G. Huang, J. Alloys Compd. 457 (2008) 560.
[15] N.J. Tang, H.Y. Jiang, W. Zhong, X.L. Wu, W.Q. Zou, Y.W. Du, J. Alloys Compd. 419 (2006) 145.
[16] X. Cao, Yu. Koltypin, R. Prozorov, G. Kataby, A. Gedanken, J. Mater. Chem. 7 (1997) 2447.
[17] J.R. Macdonald, Impedance Spectroscopy, Wiley, New York, 1987.
[18] A.K. Jonscher, Nature 267 (1977) 673.
[19] W.H. Mulder, J.H. Sluyters, T. Pajkossy, I. Nyikos, J. Electroanal. Chem. Interfacial Electrochem. 285 (1990) 103.
[20] F.D. Morrison, D.J. Jung, J.F. Scott, J. Appl. Phys. 101 (2007) 094112.

[21] J.R. Macdonald, Impedance Spectroscopy Theory, Experiment and Applications, 2nd ed., A John Wiley & Sons, Inc., New Jersey, 2005.
[22] N. Ponpandian, A. Narayanasamy, J. Appl. Phys. 92 (2002) 2770.
[23] D.P. Almond, A.R. West, Solid State Ionics 9–10 (1983) 277.
[24] J.C. Dyre, T.B. Schrøder, Rev. Mod. Phys. 72 (2000) 873.
[25] N. Guskos, E.A. Anagnostakis, V. Likodimos, T. Bodziony, J. Typek, M. Maryniak, U. Narkiewicz, I. Kucharewicz, S. Waplak, J. Appl. Phys. 97 (2005) 024304.
[26] T. Tepper, S. Berger, Nanostruct. Mater. 11 (1999) 1081.
[27] P. Chen, R.X. Wu, T. Zhao, F. Yang, J.Q. Xiao, J. Phys. D: Appl. Phys. 38 (2005) 2302.
[28] X. Zhang, T. Ekiert, K.M. Unruh, J.Q. Xiao, M. Golt, R. Wu, J. Appl. Phys. 99 (2006) 08M914.
[29] A. Verma, O.P. Thakur, C. Prakash, T.C. Goel, R.G. Mendiratta, Mater. Sci. Eng. B 116 (2005) 1.